Available online at www.sciencedirect.com
SCIENCE DIRECT
Journal of Catalysis 240 (2006) 114–125
JOURNAL OF CATALYSIS
www.elsevier.com/locate/jcat

Particle size effects on the reducibility of titanium dioxide and its relation to the water–gas shift activity of Pt/TiO_2 catalysts

P. Panagiotopoulou [a], A. Christodoulakis [a,b], D.I. Kondarides [a,*], S. Boghosian [a,b]

[a] *Department of Chemical Engineering, University of Patras, GR-26504 Patras, Greece*
[b] *Institute of Chemical Engineering and High Temperature Chemical Processes (FORTH/ICE-HT), GR-26500 Patras, Greece*

Received 8 February 2006; revised 17 March 2006; accepted 20 March 2006
Available online 24 April 2006

Abstract

The effect of primary particle size of titanium dioxide on the reducibility of Pt/TiO_2 catalysts by carbon monoxide and hydrogen was investigated using temperature-programmed reduction (TPR) techniques and in situ Raman and Fourier transform infrared spectroscopy (FTIR). Experiments were conducted over Pt catalysts supported on four commercial titanium dioxide carriers of variable structural characteristics, the water–gas shift (WGS) activity of which increases significantly with decreasing primary crystallite size of the support. TPR profiles obtained for the preoxidized catalysts using H_2 as a reductant are characterized by a low-temperature consumption peak, attributed to the reduction of PtO_x species, and a high-temperature peak, attributed to the reduction of TiO_2. The intensity of the latter peak, which is a measure of the reducibility of the support, increases drastically with increasing specific surface area of the catalyst or, conversely, with decreasing primary particle size of TiO_2. In situ Raman experiments conducted under hydrogen flow verified that formation of substoichiometric TiO_x species begins at lower temperatures and is more facile over Pt/TiO_2 catalysts with smaller titania particle sizes. The TPR profiles obtained using CO as a reductant gave qualitatively similar results, exhibiting two CO_2 peaks corresponding to reduction of PtO_x at low temperatures and of TiO_2 at high temperatures. An additional CO_2 peak located at intermediate temperatures, which was always accompanied by evolution of gas-phase H_2, is attributed to the WGS reaction. FTIR experiments indicate that the reaction occurs via interaction between CO and hydroxyl groups of the support, with intermediate formation of formates. The effect of the titanium dioxide particle size on the reducibility of Pt/TiO_2 catalysts and its relation to their WGS activity is discussed with respect to the "regenerative" and "associative" reaction mechanisms.
© 2006 Elsevier Inc. All rights reserved.

Keywords: Water–gas shift; Platinum; Titanium dioxide; Reducibility; Particle size; Temperature-programmed reduction; In situ Raman; FTIR; Hydrogen; Carbon monoxide

1. Introduction

The interest in the water–gas shift (WGS) reaction has recently increased significantly due to its potential use in fuel processors for mobile and small- to medium-sized stationary fuel cell systems [1,2]. Conventional low-temperature ($Cu/ZnO/Al_2O_3$) and high-temperature (Fe_3O_4/Cr_2O_3) WGS catalysts, which have been used in industry for several decades [3,4], cannot be used for such applications, mainly due to problems related to their narrow temperature window of operation and pyrophoricity, as well as the need for lengthy precondition steps [5]. As a result, efforts are focused on the development of novel, stable, and selective catalysts with sufficiently high activity at low temperatures, which for typical PEM fuel cell applications are in the range of 200–280 °C [2]. Oxide-supported noble metal catalysts seem to be able to meet the above criteria and thus have been widely investigated.

It is generally accepted that the WGS reaction over oxide-supported noble metal catalysts occurs in a bifunctional manner with participation of both the dispersed metallic phase and the support. In this regard, two general schemes have been proposed for the reaction [6]: (a) a redox or "regenerative" mechanism [7–13], according to which CO adsorbed on the metal is oxidized toward CO_2 by an oxygen atom of the support, which in turn is reoxidized by water, releasing hydrogen, and (b) an as-

* Corresponding author. Fax: +30 2610 991527.
E-mail address: dimi@chemeng.upatras.gr (D.I. Kondarides).

0021-9517/$ – see front matter © 2006 Elsevier Inc. All rights reserved.
doi:10.1016/j.jcat.2006.03.012

sociative mechanism [14–19], according to which the reaction proceeds via interaction of adsorbed CO with terminal hydroxyl groups of the support to form an intermediate (e.g., a formate species), which is further decomposed toward CO_2 and H_2. The applicability of the redox mechanism is by nature restricted to catalysts supported on "reducible" carriers and has been proposed to explain the high WGS activity of CeO_2-supported noble metals [7–12], as well as of Au/Fe_2O_3 and Au/TiO_2 catalysts [13]. However, Davis and co-workers [15–19] provided evidence favoring the formate intermediate mechanism on Pt/CeO_2 catalysts. In any case, most investigators agree that water adsorption and activation occur on the support, whereas carbon monoxide adsorbs on dispersed metal.

Recent studies conducted over ceria-supported gold and platinum catalysts [20–23] indicate that the role of the dispersed metallic phase is not restricted to providing sites for adsorption of CO, but that it also affects the reducibility of the support, thereby creating new active sites for the WGS reaction (oxygen vacancies within the support or partially reduced sites at the metal–support interface). Jacobs et al. [19] recognized that for Pt/CeO_2 catalysts, the partial reduction of ceria is a necessary step in both the redox and the formate mechanisms. In the formate mechanism, the reduction of the ceria surface shell is necessary to generate the bridging OH group active sites, whereas in the redox mechanism, reduction of ceria is directly involved in the reaction mechanism [19]. Although many authors have mentioned the possible effect of the reducibility of the support on the activity of WGS catalysts, this issue has not yet been investigated in detail.

In previous studies [24,25], we found that the WGS activity of supported noble metal catalysts, including Pt/TiO_2 [24], Ru/TiO_2 [24], Pt/CeO_2 [25], and Pt/Al_2O_3 [25], does not depend practically on the characteristics of the dispersed metallic phase, such as metal loading (0.1–5.0 wt%), dispersion (6–100%), and crystallite size (0.9–16.2 nm). We also found that the key parameters that determine catalytic activity are related mainly to the nature and physicochemical characteristics of the support. In particular, activity of noble metals is significantly improved when supported on "reducible" instead of on "irreducible" metal oxides [25]. We also found that the activity of Pt/TiO_2 catalysts depends strongly on the primary crystallite size of the support [24]. This was tentatively attributed to the expected higher reducibility of smaller titania crystallites, which may affect either the WGS activity either directly (redox properties) or indirectly (population and reactivity of hydroxyl groups). In the present study, we investigated the effect of primary crystallite size of titanium dioxide on the reducibility of Pt/TiO_2 catalysts using temperature-programmed reduction (TPR) and in situ Raman and Fourier transform infrared (FTIR) spectroscopy techniques.

2. Experimental

2.1. Catalyst preparation and characterization

Catalysts were prepared by the wet-impregnation method [24] using $(NH_3)_2Pt(NO_2)_2$ (Alfa) as metal precursor salt and four commercial titania powders with variable specific surface areas (SSAs) and primary particle size of TiO_2 crystallites (d_{TiO_2}) as supports. The SSAs of the as received TiO_2 powders used (see Table 1 for notations) were 238 m^2/g for UV, 159 m^2/g for PC, 41 m^2/g for P25, and 8 m^2/g for AT [24]. Impregnation was accomplished by adding the support into an aqueous solution of the metal precursor salt (pH 10) under continuous stirring. This resulted in a decrease in the solution pH in a manner depending on the nature of the TiO_2 powder added. In particular, pH did not practically change on addition of the low-surface area sample (AT), decreased to pH 8–9 on addition of P25, and decreased to pH 6–7 on addition of the high-surface area powder (UV). As discussed below, these differences affected the dispersion of platinum. The slurry was then heated slowly at 70 °C under continuous stirring and maintained at that temperature until nearly all of the water evaporated. The solid residue was subsequently dried at 110 °C for 24 h and finally reduced at 300 °C in hydrogen flow for 2 h. In all cases, the metal loading of the catalysts prepared was 0.5 wt%.

Carriers and catalysts were characterized with respect to their SSA, TiO_2 crystallite size, and platinum dispersion, using nitrogen physisorption at the temperature of liquid nitrogen, X-ray diffraction (XRD), and selective chemisorption of H_2, respectively [24]. Results of the characterization of fresh catalysts are summarized in Table 1. The relatively low dispersion of Pt obtained for the high-surface area samples (UV and PC) can be understood by taking into account the fact that dispersion is strongly affected by the experimental conditions used during preparation (e.g., solution pH), by the characteristics of the metal oxide support (e.g., zero point of charge [ZPC]), and by the interaction between the metal precursor and the support. For example, if the pH value of the slurry is changed, then both the surface charge of TiO_2 and the adsorption of metal ions will be influenced. The relatively low Pt dispersion obtained for the high-surface area TiO_2 carrier (UV) is most probably due to the

Table 1
Results of characterization of fresh and conditioned[a] 0.5% Pt/TiO_2 catalysts (reproduced from [24])

Type of TiO_2 support (producer)	Notation	TiO_2 phase composition (%anatase)	Primary TiO_2 crystallite size, d_{TiO_2} (nm)	Specific surface area (SSA) (m^2/g)	Pt dispersion (%)
PC-500 (Millennium Chemicals)	Pt/PC	100	11 (18)	111 (64)	62
Hombikat UV-100 (Sachtleben Chemie)	Pt/UV	100	12 (16)	104 (71)	14
P-25 (Degussa)	Pt/P25	75	25 (25)	41 (39)	87
AT-1 (Millennium Chemicals)	Pt/AT	100	33 (35)	8 (8)	47

[a] Values in parentheses correspond to the "conditioned" samples, i.e., catalysts heated for 15 min in He flow at 500 °C followed by exposure to a 3% CO–10% H_2O (in He) reaction mixture at 450 °C for 1 h.

fact that the pH of the slurry (pH 6–7) was in this case very close to the ZPC of TiO_2. Under these conditions, the oxide particles are not charged, and they tend to agglomerate, thereby resulting in a decrease in the surface area available for adsorption and deposition of the metal ions. In contrast, the pH of the slurries containing the low surface area TiO_2 powders (AT and P25) was much higher (>8) than the ZPC of TiO_2. As a result, TiO_2 particles were very well dispersed in the slurry due to the presence of repulsive electrostatic forces, and practically all of the surface area of the support was available for adsorption/deposition of Pt ions. Optimization of the catalyst preparation method to increase metal dispersion was beyond the scope of the present study and thus was not investigated further.

Table 1 also gives characterization results obtained from the "conditioned" samples (values in parentheses), that is, after heating the freshly prepared catalysts at 450 °C in He flow for 15 min and subsequent exposure to a 3% CO–10% H_2O (in He) mixture for 1 h at 450 °C (see below). It can bee seen that conditioning results in a decrease of SSA and an increase of d_{TiO_2}, which is more pronounced for the high-surface area samples (Pt/PC and Pt/UV) and less significant or negligible for the low-surface area samples (Pt/P25 and Pt/AT) (Table 1).

2.2. Kinetic measurements

The catalytic activity of Pt/TiO_2 catalysts for the WGS reaction was investigated using an apparatus and following the procedures described in detail elsewhere [24]. Briefly, the apparatus consisted of a set of mass-flow controllers (MKS) to control the flow and composition of the inlet gases (CO, H_2, and He); a syringe pump (Braintree Scientific) connected to an evaporator, which is used for feeding steam; and a set of valves that allow selection of gas feed composition and introduction of the gas mixture to the reactor or to a bypass loop stream. The analysis system consists of a gas chromatograph (Shimadzu) equipped with two packed columns (Porapak-Q, Carboxen) and two detectors (thermal conductivity and flame ionization detectors), operating with He as the carrier gas. Determination of the response factors of the detectors is achieved using gas streams of known composition (Scott specialty gas mixtures). Gases (He, 10% CO/He, H_2) are supplied from high-pressure gas cylinders (Messer Griesheim GMBH) and are of ultra-high purity.

In a typical experiment, a preweighted amount (60–100 mg) of fresh catalyst ($0.18 < d < 0.25$ mm) is placed in the reactor and reduced in situ at 300 °C for 1 h under a hydrogen flow of 60 cc/min. The catalyst is then heated at 500 °C under He flow, maintained at that temperature for 15 min, and finally conditioned by exposure to the reaction mixture (3% CO–10% H_2O in He) at 450 °C for 1 h. Measurements of reaction rates were then obtained under conditions with the conversion of reactants <10%, by varying the mass of catalyst and/or the flow rate. Rates were calculated using the following expression:

$$r_{CO} = \frac{(C_{CO}^{in} - C_{CO}^{out})F}{W}, \quad (1)$$

where r_{CO} is the conversion rate of CO (mol/(s g_{cat})), F is the total flow rate (mol/s), W is the mass of catalyst (g), and C_{CO}^{in} and C_{CO}^{out} are the inlet and outlet concentrations of CO, respectively. Results of kinetic measurements and Pt dispersion were used to determine the turnover frequencies (TOFs) of carbon monoxide consumption, defined as mol of CO converted per surface noble metal atom per second (see Ref. [24] for details). All experiments were performed at near-atmospheric pressure.

2.3. TPR experiments

TPR experiments were carried out using either hydrogen (H_2-TPR) or carbon monoxide (CO-TPR) as a reducing agent, using an apparatus and following the procedure described elsewhere [26,27]. In a typical experiment, 200 mg of the catalyst was placed in a quartz microreactor and treated at 300 °C with a flowing 2% O_2/He mixture (40 cm^3/min) for 30 min. The sample was then heated under He flow (40 cm^3/min) at 500 °C for 15 min to remove adsorbed species from the catalyst surface and subsequently cooled at room temperature. TPR experiments were then carried out by switching the feed composition from He to 0.5% H_2/He or 0.25% CO/He (40 cm^3/min), maintaining it at 25 °C for 10 min, and then heating linearly ($\beta = 30$ °C/min) at 650 °C. Analysis of gases at the effluent of the reactor was done using an on-line mass spectrometer (Fisons, SPX Elite 300 H) equipped with a fast-response inlet capillary/leak diaphragm system. The transient-MS signals at $m/z = 2$ (H_2), 15 (CH_4), 18 (H_2O), 28 (CO), and 44 (CO_2) were recorded continuously. Where necessary (e.g., for CO_2–CO signals), the cracking coefficient determined in separate experiments was also taken into account in the calculations. Calibration of the mass spectrometer was done based on self-prepared gas mixtures of accurately known composition.

2.4. In situ Raman spectroscopy

An appropriate homemade in situ Raman reactor cell was used to monitor the Raman spectra of the catalyst samples studied under various conditions. The reactor cell, which had a gas inlet and a gas outlet as well as an entrance to accommodate a T/C sheath, was composed of quartz and had a quartz frit for holding the catalysts in place in a fixed bed. Approximately 150 mg of each catalyst sample in the form of powder with particle sizes 125–250 μm in diameter were loaded in the quartz reactor cell. The reactor cell was mounted in vertical position inside a kanthal-wound double-walled quartz-glass transparent tube furnace mounted on a xyz plate that enabled it to be positioned on the optical table. Temperature was controlled and measured by a thermocouple inserted in an appropriate quartz sheath, which was in contact with the catalyst bed. The gases used were O_2 (L'Air-Liquide 99.999%) and a 4.3% H_2/N_2 mixture (L'Air-Liquide). The gas flow was controlled by electronic thermal mass flow meters.

The 514.5-nm line of a Stabilite 2017 Ar^+ laser (Spectra Physics), operated at a power level of 120 mW at the sample, was used to record the Raman spectra. To reduce irradiance on

the samples, the laser light was dispersed by slightly defocusing the incident beam. The scattered light was collected at 90° (horizontal scattering plane), analyzed with a 0.85 Spex 1403 double spectrometer, and detected by a −20 °C cooled RCA photon multiplier equipped with EG&G photon counting electronics.

Before recording in situ Raman spectra, each sample was treated in flowing O_2 for 1 h at 300 °C, then cooled at room temperature to record the spectrum of the oxidized catalyst. Subsequently, in situ Raman spectra were obtained in reducing atmosphere under flowing 4.3% H_2/N_2 in the 25–450 °C range by studying the temperature dependence of the spectra in 100 °C intervals. At each temperature, the catalyst sample was exposed to the flowing gas for 1 h before the spectra were recorded.

2.5. In situ FTIR spectroscopy

A Nicolet 740 FTIR spectrometer equipped with a diffuse reflectance Fourier transform infrared spectroscopy (DRIFTS) cell, an MCT detector, and a KBr beam splitter was used [26,27]. FTIR spectra were collected with a 64-scan data acquisition at a resolution of 4 cm^{-1} in a controlled gas atmosphere and temperature using a DRIFTS cell (Spectra Tech). During measurements, the external optics were purged with dry air to minimize the level of atmospheric water vapor and CO_2. The cell was directly connected to a flow system equipped with mass flow controllers and a set of valves that allowed selection of feed gas composition.

In a typical experiment, the catalyst in finely powdered form was placed into the sample holder, and its surface was carefully flattened to increase the intensity of the reflected IR beam. The catalyst sample was first heated under flowing He at 450 °C for 10 min, followed by oxidation with 10% O_2/He at 300 °C for 30 min. The oxidized sample was then heated at 450 °C under He flow for 15 min and subsequently cooled to room temperature. In the cooling stage, background spectra were collected at temperatures of interest. Finally, the flow was switched to 1% CO/He, and the first spectrum was recorded at room temperature after 10 min on stream. The temperature was then increased in a stepwise mode up to 450 °C, and spectra were obtained at selected temperatures after equilibration for 10 min on stream. After recording the spectrum, the temperature was increased to the next selected temperature. In all experiments, the total flow through the DRIFTS cell was 30 cm^3/min.

3. Results and discussion

3.1. WGS activity of Pt/TiO_2 catalysts

Results of kinetic measurements obtained from the four Pt/TiO_2 catalysts investigated are summarized in the Arrhenius-type diagram of Fig. 1. It can be seen that the reaction rate depends strongly on the type of TiO_2 carrier used and increases with increasing surface area of the support or, conversely, with decreasing the primary particle size of TiO_2 (Table 1). In particular, the rate at 250 °C increases by a factor of 20 going from Pt/AT (1.2 μmol/(g s)) to Pt/UV (24.0 μmol/(g s)) catalyst, that is, by decreasing d_{TiO_2} from 35 to 16 nm (with values corresponding to the conditioned samples). These differences become more pronounced when comparing the TOFs determined for the above samples, in which case the rate per surface Pt atom is found to differ by more than two orders of magnitude [24]. It is of interest to note that the apparent activation energy (E_a) of the reaction also varies depending on the TiO_2 support used, decreasing from 16.9 kcal/mol for the Pt/AT catalyst to 11.9 kcal/mol for the Pt/UV catalyst (Fig. 1) [24].

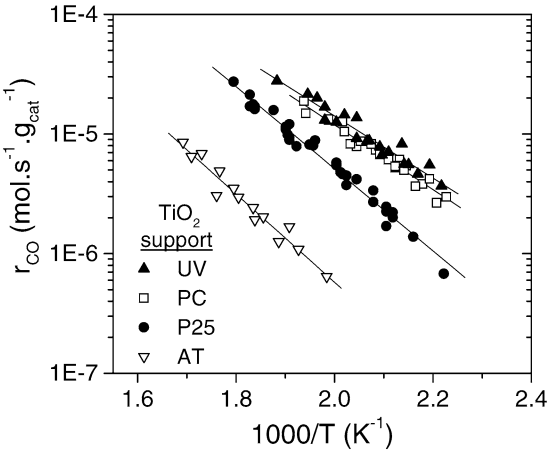

Fig. 1. Arrhenius plots of WGS reaction rates obtained from Pt catalysts (0.5 wt%) supported on the indicated TiO_2 carriers.

3.2. TPR with H_2

Hydrogen-TPR profiles obtained from the preoxidized Pt/TiO_2 catalyst samples are shown in Fig. 2. It can be seen that in the case of Pt supported on AT [i.e., the support with the lowest surface area (largest d_{TiO_2})], two hydrogen consumption features are present. Trace a exhibits a low-temperature (LT) peak with maximum at ca 190 °C and a high-temperature (HT) broad feature evolving at temperatures above 350 °C and present up to 650 °C, at which point the experiment was stopped. Qualitatively similar results were obtained over Pt/P25 (trace b), a catalyst with higher surface area (lower d_{TiO_2}) than Pt/AT. Here, however, both the LT and, especially, the HT consumption peaks increase in intensity, with the latter shifting toward lower temperatures. The same trend was also observed on further increasing the SSA (decreasing d_{TiO_2}) of the Pt/TiO_2 catalyst, as shown in the H_2-TPR spectra obtained from the Pt/UV (trace c) and Pt/PC (trace d) samples. In these latter two catalysts, the HT reduction peak begin to evolve at temperatures below 300 °C and exhibit a clear maximum in the range of 410–440 °C. Comparing the hydrogen consumption curves in Fig. 2 with the structural and morphological characteristics of Pt/TiO_2 samples (Table 1) clearly shows that the reducibility of the catalyst increases with increasing SSA or, equivalently, with decreasing primary crystallite size of TiO_2.

Previous studies conducted over supported Pt catalysts have shown that oxidation of Pt crystallites dispersed on TiO_2,

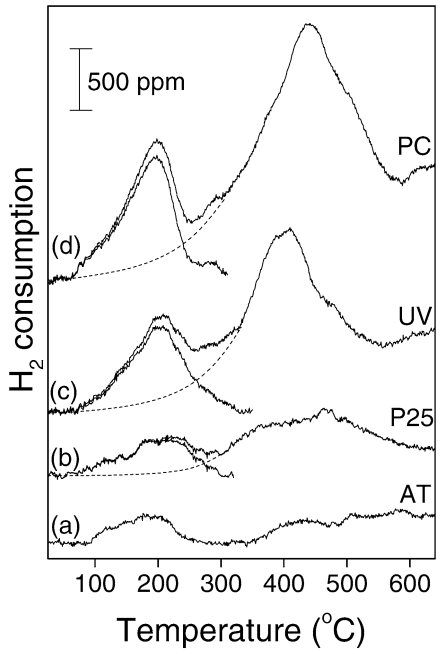

Fig. 2. Hydrogen-TPR profiles obtained from the preoxidized Pt/TiO_2 catalysts. Experimental conditions: total flow = 40 cm^3/min (0.5% H_2/He); $\beta = 30\,^{\circ}C$/min.

Al_2O_3, CeO_2, and their mixtures results in the formation of various platinum oxides [28–31], including Pt_sO (surface platinum oxide), PtO, and PtO_2, with these species alternating with increasing oxidation temperature from 25 to 500 °C [30]. In H_2-TPR experiments, these species are reduced at temperatures below 250 °C, with the exact reduction temperature depending on the degree of crystallinity of the Pt oxide; the more crystalline the oxide, the lower the reduction temperature [31]. It may then be suggested that pretreating the present samples under a flowing 2% O_2/He mixture at 300 °C before the TPR experiments resulted in the formation of such oxide species (PtO_x). Part of the so-formed PtO_x probably is decomposed during subsequent thermal treatment at 500 °C under He flow. For example, bulk PtO_2 is known to decompose at temperatures around 300 °C [28]. However, PtO_2 is stabilized when dispersed on Al_2O_3, TiO_2, or SiO_2, due to interactions with the support, and decomposes at substantially higher temperatures [28].

Based on the above discussion, it may be argued that pretreatment of Pt/TiO_2 catalysts applied in the present study resulted in the formation of PtO_x species, part of which were present on the catalyst before the H_2-TPR experiments. On heating in H_2/He flow, PtO_x particles were reduced at temperatures below 250 °C [28–31] according to the following equation:

$$PtO_x + xH_2 \rightarrow Pt + xH_2O. \quad (2)$$

Therefore, the LT consumption peak observed for all samples investigated, with its maximum located at ca. 200 °C (Fig. 2), is attributed to reduction of PtO_x.

The chemical composition of the PtO_x species may be estimated according to the stoichiometry of Eq. (2) from the ratio N_{H_2}/N_{Pt}, where N_{H_2} denotes the number of hydrogen molecules consumed and N_{Pt} denotes the number of Pt atoms contained in each sample. For this, the LT peak was deconvoluted as shown schematically in the H_2-TPR curves of Fig. 2, and N_{H_2} was determined for each sample. Results are summarized in Table 2, along with the calculated N_{H_2}/N_{Pt} ratios. It can be seen that the degree of Pt oxidation depends on the nature of the titania support used and increases with increasing (decreasing) surface area (primary crystallite size) of TiO_2. The calculated N_{H_2}/N_{Pt} ratios for Pt/AT and Pt/P25 catalysts correspond to surface oxidation of Pt crystallites, whereas in the case of Pt/UV and Pt/PC samples, oxidation is not restricted to the crystallite surface, but also involves oxidation of the core of the dispersed Pt crystallites.

Table 2
Hydrogen consumption related to the reduction of Pt oxides and TiO_2 and estimation of the chemical composition of PtO_x particles and degree of reduction of titania. Data obtained from the deconvoluted H_2-TPR profiles of Fig. 2

	Low-temperature peak (reduction of PtO_x)		High-temperature feature (reduction of TiO_2)	
	H_2 consumption (μmol H_2/g)	N_{H_2}/N_{Pt} ratio ("x" in PtO_x)	H_2 consumption (μmol H_2/g)	O/Ti ratio ("x" in TiO_x)
Pt/AT	7.2	0.28	21.0	1.998
Pt/P25	11.2	0.43	36.6	1.997
Pt/UV	29.5	1.15	81.5	1.993
Pt/PC	23.6	0.92	158.8	1.987

The observed differences in the stoichiometry of PtO_x particles with increasing (decreasing) surface area (d_{TiO_2}) (see Table 2) may be attributed to a different extent of interaction of platinum with the support. It may be suggested that increasing SSA (decreasing d_{TiO_2}) results in a higher propensity of dispersed Pt to be oxidized after interaction of the metal with O_2/He at 300 °C during the pretreatment step. Alternatively, it is possible that PtO_x species formed during this preoxidation step are decomposed more easily on subsequent heating at 500 °C under He flow, when supported on low-surface area (large d_{TiO_2}) titania supports. However, catalyst characteristics other than SSA or d_{TiO_2} also may be responsible for the observed differences in the stoichiometry of the PtO_x particles, including Pt dispersion. Investigating the origin of this effect is beyond the scope of the present investigation and is not discussed further.

Regarding the HT hydrogen consumption feature observed in the TPR experiments shown in Fig. 2, it can be proposed that this may be related to the Pt-catalyzed reduction of the support. It is well known that titanium dioxide is partially reduced to TiO_{2-x} by hydrogen at high temperatures (above 500 °C), according to the following equation:

$$TiO_2 + xH_2 \rightarrow TiO_{2-x} + xH_2O \quad (x < 2). \quad (3)$$

The process is promoted by the presence of dispersed metal crystallites and is believed to be at the origin of the SMSI effect [32,33]. Results of ESR and NMR measurements show that indeed Ti^{3+} ions are formed when Pt/TiO_2 is reduced even at temperatures below 250 °C [34–36]. It has been proposed that dispersed Pt promotes reduction of TiO_2 via the formation of

dissociatively adsorbed hydrogen atoms, which diffuse to the support and reduce Ti^{4+} ions to Ti^{3+} according to [28],

$$Ti^{4+} + O^{2-} + H_{(ads)} \rightarrow Ti^{3+} + OH^{-}. \quad (4)$$

At low temperatures (<250 °C), only Ti^{4+} ions close to the metal particles at the surface of the TiO_2 are reduced, whereas at higher temperatures other Ti^{4+} ions also can be reduced [28,35].

Returning to the H_2-TPR profiles of Fig. 2, it is evident that the intensity of the HT feature, attributed to reduction of TiO_2, increases significantly with increasing the surface area (decreasing d_{TiO_2}) of the support, accompanied by a shift in the onset of the reduction toward lower temperatures. The extent of the reduction of the support at the end of the H_2-TPR experiments was estimated for all samples investigated from the area below the corresponding HT peaks; the results are listed in Table 2. Clearly, the reducibility of titanium dioxide, expressed by the calculated value of x in TiO_x (Table 2), depends strongly on the primary crystallite size of titania and increases significantly with decreasing d_{TiO_2}. This finding is in agreement with calculations of Cordatos et al. [37], who showed that the reducibility of small oxide clusters depends on their size, as has been found for, for example, ceria [7,37] and lanthana [38]. In the case of ceria, in which the effect of particle size on reducibility is much more pronounced and widely studied [39,40], a lower reduction enthalpy of high-surface area samples compared with that of the bulk material, has been reported [41].

3.3. In situ Raman spectra

The effect of the morphological properties of the support on the reducibility of Pt/TiO_2 catalysts was further investigated using Raman spectroscopy. Fig. 3 shows the Raman spectra of all samples studied under flowing O_2 at room temperature, obtained after the catalysts were subjected to oxidation at 300 °C for 1 h. The Raman spectrum obtained for the empty quartz reactor cell is included for comparison (spectrum a in Fig. 3); depending on the signal obtained for each studied sample, bands due to vitreous SiO_2 may or may not be recognized in the Raman spectra. At any case, as clearly seen in, for example, spectrum b (Fig. 3) obtained from the Pt/UV sample, Raman scattering from the quartz reactor is responsible for the lifted background in the 425–500 cm^{-1} region; likewise the 485 cm^{-1} feature in spectrum e (Fig. 3) is due to vitreous SiO_2 and becomes prominent due to the weak intensity of the TiO_2 bands from sample Pt/AT. The Raman spectra shown in Fig. 3 exhibit the well-known TiO_2-anatase bands at 398, 516, and 640 cm^{-1} for all samples studied plus the two characteristic TiO_2-rutile bands at 612 and 447 cm^{-1} for the Pt/P25 sample, which contains 25% TiO_2-rutile (see Table 1). The spectra are recorded with the same conditions (e.g., photon accumulation time, laser power, optical geometry), and the relative intensities of each spectrum reflect the population (amplitude) of TiO_2 particles illuminated in the laser irradiation spot; as expected, the overall Raman signal decreases in the sequence UV > PC > P25 ≫ AT, in agreement with the decreasing values for the sample-SSA along the series.

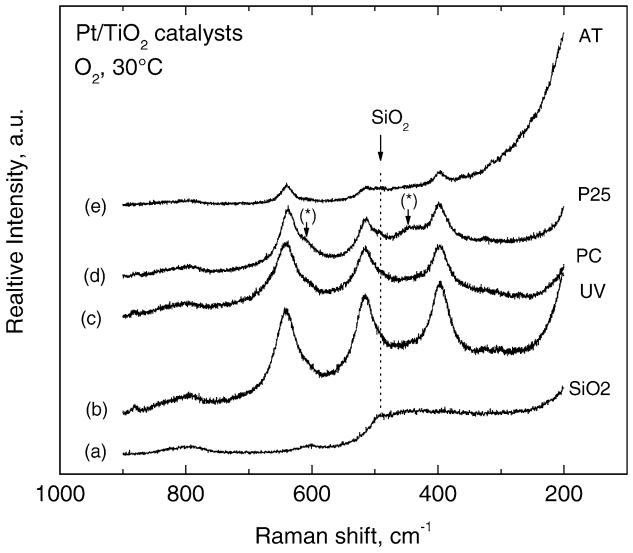

Fig. 3. Raman spectra (b–e) of preoxidized Pt/TiO_2 catalysts recorded under O_2 at 30 °C. The spectrum of the empty quartz reactor is included for comparison (spectrum a). Bands due to titania–rutile are marked by (*). Laser wavelength, $\lambda_0 = 514.5$ nm; laser power, $w = 120$ mW; scan rate, sr = 0.08 − 0.1 cm^{-1}/s, time constant, $\tau = 4$ s; spectral slit width, ssw = 6 cm^{-1}.

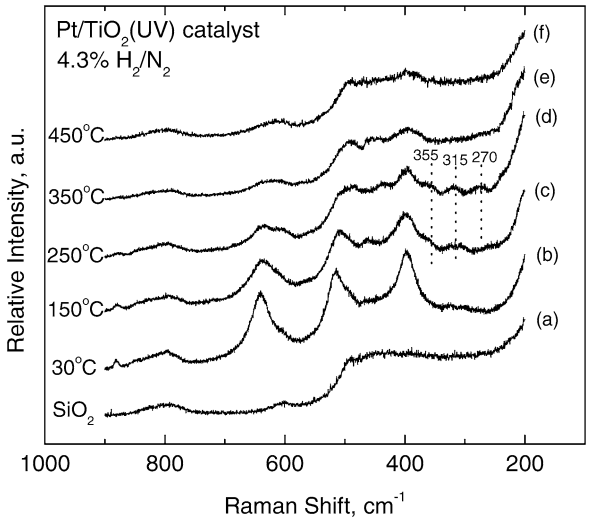

Fig. 4. In situ Raman spectra of Pt/TiO_2(UV) catalyst recorded under H_2/N_2 atmosphere at temperatures as indicated by each spectrum. Recording parameters: see Fig. 3 caption.

Fig. 4 shows the temperature dependence of the in situ Raman spectra obtained in flowing 4.3% H_2/N_2 gas in the 25–450 °C range for the representative sample Pt/UV, which exhibited the highest TOF for the WGS reaction (Fig. 1). The other samples exhibited *mutatis mutandis* analogous behavior. In situ Raman spectra were recorded sequentially after the sample was exposed to H_2-containing flowing gas for 1 h at each temperature. The Raman spectrum under hydrogen at room temperature (Fig. 4b) is almost identical to the spectrum b (Fig. 3) obtained for the oxidized sample. It is evident that at 150 °C (Fig. 4c) the anatase bands already start losing intensity and become broader, and new, weak bands appear in the 270–355 cm^{-1} and 460 cm^{-1} region. The intensity loss of the anatase bands

is attributed to reduction by H_2, resulting in a decreased O/Ti ratio and formation of substoichiometric titania phases. A decreased O/Ti ratio and formation of substoichiometric titania phases are also responsible for the progressive broadening of the bands [42], an effect that is further intensified by thermal broadening with increasing temperature.

The weak bands in the 260–360 cm^{-1} region and the 460 cm^{-1} band gain intensity on going from 150 °C (spectrum c in Fig. 4) to 250 °C (spectrum d in Fig. 4) and are indicative of Ti_2O_3 formation, which is formed at the expense of TiO_2-anatase, of which the bands progressively decrease in intensity with increasing temperature in hydrogen atmosphere. The Raman spectra of Ti_2O_3 are known from studies of single crystals [43,44]; it has been reported that both the position and the intensity of the most prominent Ti_2O_3 bands are temperature-sensitive due to rapid changes in the physical properties (e.g., the lattice parameters) of this material over a range of 150 °C starting in the vicinity of 125 °C [43]. Moreover, the shape and the broadness of the Ti_2O_3 bands vary with the degree of crystallinity; broad bands in the same region have been imputed to amorphous Ti_2O_3 [45,46].

With a further temperature increase to 350 °C (Fig. 4e), the Ti_2O_3 bands disappear, and only weak contributions from the remaining TiO_2-anatase bands can be observed superimposed on the broad SiO_2 features due to scattering of the incident laser from the walls of the quartz reactor cell. It is evident that with further reduction and oxygen removal from the multiple titania phases, TiO and Ti_2O may form; however, these two phases are not Raman active [46,47], and thus after catalyst surface is exposed to H_2 at 450 °C for 1 h, the titania phases become Raman silent (Fig. 4, spectrum f).

Fig. 5 compares the behavior of various Pt/TiO_2 catalyst samples under hydrogen at constant temperature. Fig. 5A shows the in situ Raman spectra obtained for the Pt/UV, Pt/PC, and Pt/P25 samples under H_2/N_2 at 150 °C, and Fig. 5B shows the corresponding spectra obtained at 250 °C. The following statements regarding the spectra of Fig. 5 can be made: (a) Already at 150 °C formation of Ti_2O_3 occurs at the surface of the UV sample (spectrum a in Fig. 5A), as evidenced by the presence of the characteristic weak bands in the 270–360 cm^{-1} region; (b) no new bands appear for the Pt/PC and Pt/P25 samples at 150 °C (spectra b and c in Fig. 5A), but the anatase bands lose much of their intensity compared with the spectra in Fig. 3 obtained for the oxidized respective samples, and furthermore, the bands broaden, and the same occurs for the TiO_2-rutile bands (marked by asterisks) exhibited in the spectra of Pt/P25, presumably due to lowering of the O/Ti ratio [42] due to the removal of oxygen; (c) at 250 °C (Fig. 5B), the formation of Ti_2O_3 is evidenced in all three samples and appears to proceed at the expense of the TiO_2 phases (compare, e.g., spectra a, Figs. 5A and 5B and spectra b, Figs. 5A and 5B); (d) the extent of reduction is larger for the Pt/UV sample, which has the highest SSA and the lowest initial TiO_2 crystal particle size. The last conclusion is reached after considering that formation of Ti_2O_3 is first detected for the Pt/UV sample at 150 °C, whereas at 250 °C the formation of Ti_2O_3 is more extensive for Pt/UV than for Pt/PC and Pt/P25 (Fig. 5B); furthermore, the intensity loss is

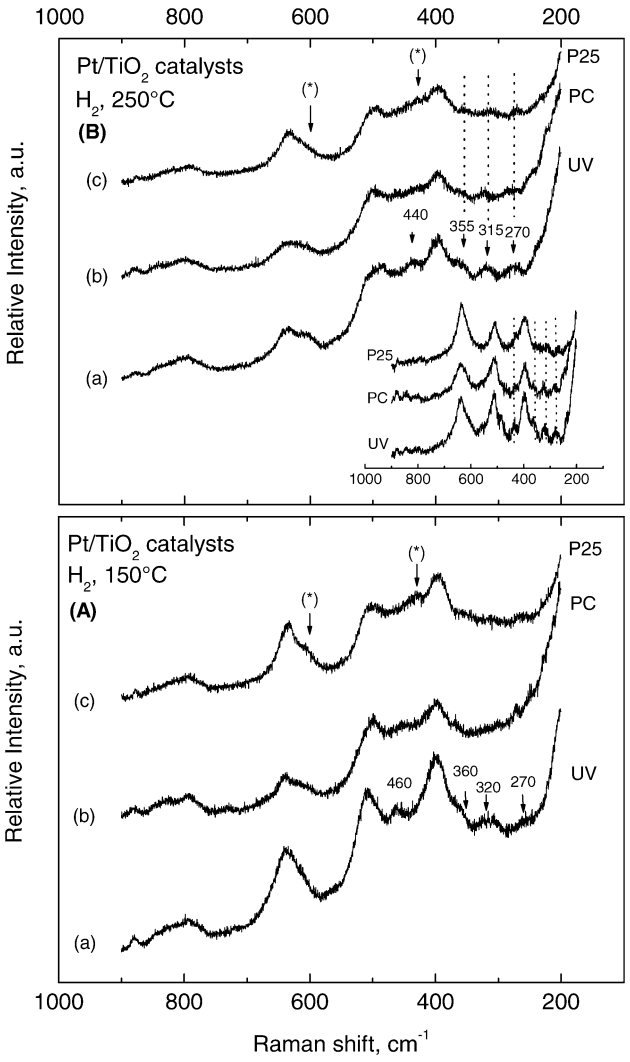

Fig. 5. In situ Raman spectra of Pt/TiO_2(UV, PC, and P25) catalysts under H_2/N_2 atmosphere: (A) at 150 °C; (B) at 250 °C. The inset shows the spectra at 250 °C after subtraction of the spectrum of the SiO_2-reactor. Bands due titania–rutile are marked by (*). Recording parameters: see Fig. 3 caption.

more abrupt for the TiO_2-anatase bands than for all other samples. Thus, whereas in an oxidized state (as shown in Fig. 3), the TiO_2-anatase bands are stronger for Pt/UV and decrease in the sequence UV > PC > P25 > AT, as explained above, in a reducing atmosphere the Pt/UV sample undergoes a relatively easy reduction with increasing temperature, as shown in Fig. 4. At 250 °C (as shown in Fig. 5B), a considerable amount of Ti_2O_3 is present in the UV sample, and the amount of detectable anatase is now almost equal for the studied samples. This is most clearly shown in the inset of Fig. 5B, where an attempt is made to subtract the contribution of SiO_2 from the spectra of Fig. 5B. Actually, Pt/UV and Pt/PC samples have undergone reduction to an extent that results in equal or lower presence of detectable TiO_2-anatase for Pt/UV and Pt/PC compared with Pt/P25. With further increases in temperature, the reduction is much more extensive for the samples with high surface areas (see, e.g., Fig. 4 for the UV sample), and finally, at 450 °C, the Raman band intensities due to anatase increase in the sequence AT ≫ P25 > PC > UV, in agreement with an increasing

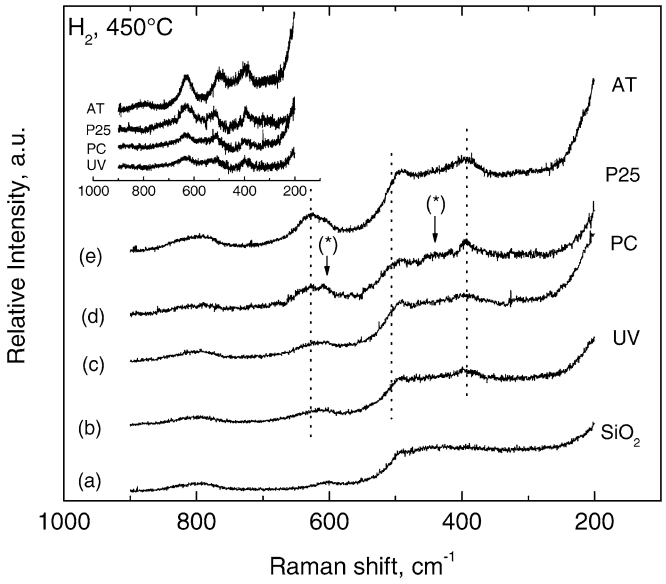

Fig. 6. In situ Raman spectra of Pt/TiO_2(UV, PC, P25, and AT) catalysts under H_2/N_2 atmosphere at 450 °C. Dotted lines mark the positions of the main titania-anatase bands. Bands due titania–rutile are marked by (*). The inset shows the corresponding spectra after subtraction of the spectrum of the SiO_2-reactor. Recording parameters: see Fig. 3 caption.

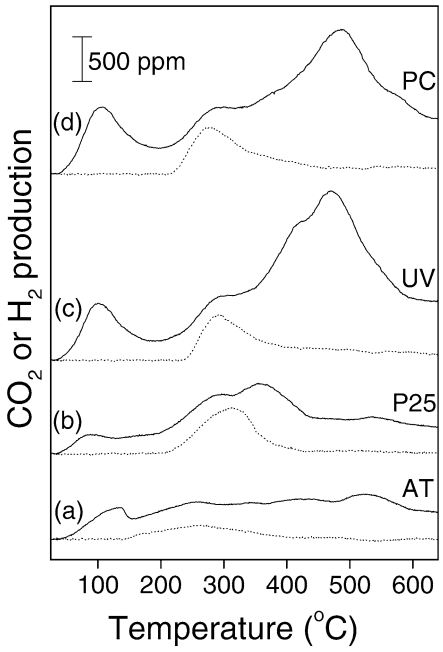

Fig. 7. Responses of CO_2 (—) and H_2 (···) obtained during TPR of preoxidized Pt/TiO_2 catalysts with 0.25% CO/He. Experimental conditions: Total flow = 40 cm^3/min; $\beta = 30$ °C/min.

reducibility of the carrier in the same sequence, which is also demonstrated by the H_2-TPR measurements (Fig. 2). This is shown in Fig. 6 depicting the in situ Raman spectra obtained for all samples in H_2/N_2 atmosphere at 450 °C. The inset in Fig. 6 shows the Raman spectra after subtraction of the SiO_2 spectrum.

3.4. TPR by carbon monoxide

Because the reducibility of the present Pt/TiO_2 catalysts is investigated with respect to their WGS activity, TPR experiments were also conducted using CO as the reducing agent. The results are summarized in Fig. 7, in which the responses of CO_2 and H_2 produced are plotted as functions of temperature. It can be seen that in all cases, the CO_2 profiles consist of an LT peak with its maximum located at 90–120 °C, a HT broad feature evolving above ca. 350 °C, and a medium-temperature (MT) shoulder, which appears at temperatures around 300 °C (Fig. 7). The intensities of the LT and HT CO_2 peaks increase with increasing surface area (decreasing d_{TiO_2}) of the support in a manner that is qualitatively similar to that observed in the H_2-TPR experiments (Fig. 2) and thus may be attributed to reduction of platinum oxide and TiO_2, respectively:

$$PtO_x + xCO \rightarrow Pt + xCO_2 \quad (5)$$

and

$$TiO_2 + xCO \rightarrow TiO_{2-x} + xCO_2 \quad (x < 2). \quad (6)$$

The MT CO_2 shoulder is always accompanied by evolution of hydrogen in the same temperature range (Fig. 7), indicating that CO_2 and H_2 are products of the same surface process. Because the only source of hydrogen under the present experimental conditions is the population of hydroxyl groups on the support, the simultaneous evolution of CO_2 and H_2 can be attributed to the WGS reaction [48–50],

$$CO_{(ads)} + 2OH^-_{(support)} \rightarrow CO_{2(g)} + H_{2(g)} + O^{2-}_{(support)}. \quad (7)$$

The reaction probably occurs at the metal–support interface between CO adsorbed on the metal and hydroxyl groups associated with the support.

Another possible route for CO_2 production under the present conditions is disproportionation of CO according to the reaction

$$2CO \rightarrow C + CO_2. \quad (8)$$

However, previous CO-TPR studies over Pt/Al_2O_3 [48,51], $Pt/Al_2O_3/CeO_2$ [48], and $Pd/CeO_2/TiO_2$ [50] catalysts showed that the contribution of this reaction to the TPR responses of CO_2 is negligible, and thus we do not discuss this further here.

The CO-TPR results of Fig. 7 clearly show that, like hydrogen (Fig. 2), carbon monoxide is able to reduce titania and that the reducibility of TiO_2 increases drastically with increasing surface area (decreasing d_{TiO_2}) of the support. It is of interest to note that reduction of PtO_x occurs at sufficiently lower temperatures (90–120 °C) when CO is used as a reductant (Fig. 7) compared to when H_2 is used as a reductant (∼200 °C) (Fig. 2).

3.5. FTIR investigation of the interaction of Pt/TiO_2 catalysts with CO

Representative DRIFTS spectra obtained from the preoxidized Pt/PC catalyst after interaction with a flowing 1% CO/He mixture at 25 °C and subsequent stepwise heating at 450 °C are shown in Fig. 8. It can be seen that the spectrum recorded at 25 °C (trace a) is characterized by bands located at 3603, 1579, and 1435 cm^{-1}, which are due to carbonate-like species associated with the support [13,52–54] and by bands in the ν(CO)

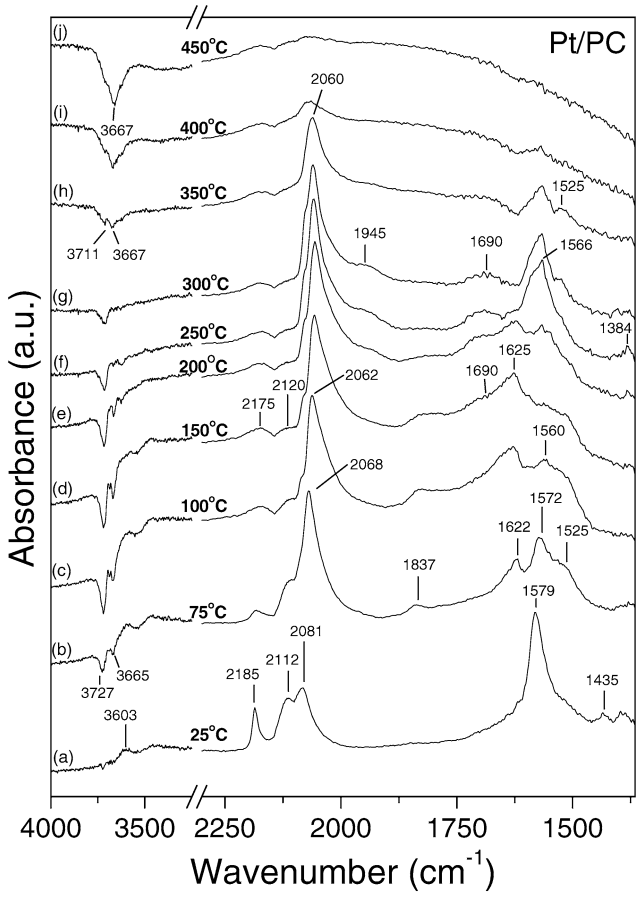

Fig. 8. DRIFT spectra obtained from the preoxidized Pt/TiO_2(PC) catalyst following exposure to 1% CO/He for 10 min at 25 °C and stepwise heating at 450 °C.

region located at 2185, 2112, and 2081 cm^{-1}. The band located at 2185 cm^{-1}, which disappeared on switching to He for 5 min (spectrum not shown) or on increasing temperature to above 75 °C (Fig. 8), may be safely attributed to CO adsorbed on weak Lewis acid sites of the support (β sites), namely Ti^{4+}–CO [55,56]. The band at 2112 cm^{-1} appears at wavenumbers corresponding to CO adsorbed either on reduced sites of anatase TiO_2 (γ sites), namely Ti^{3+}–CO [55], or on platinum(II) oxide [57–59]. The intensity of the Ti^{3+}–CO band is generally of much lower intensity compared with that of Ti^{4+}–CO, which is not the case here. Based on this observation, and taking into account that the present spectrum was obtained from the preoxidized sample, the 2112-cm^{-1} band is assigned to CO adsorbed on PtO. The band at 2081 cm^{-1} corresponds to vibrational frequencies higher than those expected from CO adsorbed on reduced platinum sites (see below) and, in agreement with results in the literature [58,59], is attributed to CO adsorbed on partially oxidized platinum ($Pt^{\delta+}$–CO).

Increasing temperature to 75 °C (trace b) and 100 °C (trace c) under flowing CO/He mixture results in the progressive disappearance of the bands corresponding to CO adsorbed on PtO (2112 cm^{-1}) and $Pt^{\delta+}$ (2081 cm^{-1}). (Note that the remaining weak, broad bands located at 2175 and 2120 cm^{-1}, which are present in all spectra, are due to gas-phase CO.) This is paralleled by the development of bands located at 2068 and 1837 cm^{-1}, which are characteristic of linear and bridge-bonded CO on reduced platinum sites (Pt^0), respectively [49,57–60]. These results clearly show that reduction of PtO_x species by CO is accomplished at temperatures around 100 °C, in agreement with the CO-TPR results (Fig. 7, trace d).

Further increases in temperature result in a progressive decrease of the intensity of the 1837 cm^{-1}-band, attributed to bridged CO, which disappears above 200 °C (traces d–f). The band attributed to linear CO is thermally more stable and disappears from the spectrum at temperatures above 400 °C (traces i and j). This is accompanied by a progressive red shift of the 2068 cm^{-1} band to 2060 cm^{-1}, which is consistent with a decrease in the dipole–dipole coupling effect between adsorbed CO molecules with decreasing coverage [57–60].

It is of interest to note that a new band appears in the ν(CO) region on heating at temperatures above 150 °C, located at ca. 1945 cm^{-1}, which is present in the spectra obtained in the temperature range of 200–350 °C (traces d–h). The low frequency of this band, which cannot be solely explained by a decrease in dipole–dipole coupling (e.g., adsorption on isolated platinum sites) may be attributed to CO species adsorbed on platinum with increased electron density. Primet [58] showed that chemisorption of electron donor compounds results in a substantial decrease of the ν(CO) frequency due to electron transfer toward platinum, which increases the back-donation of the metal electrons into the $2\pi^*$ antibonding orbitals of adsorbed CO. Results of TPR and Raman experiments (Figs. 2–7) discussed above clearly demonstrate that above 150 °C, where the 1945-cm^{-1} band starts to develop, reduction of the titanium dioxide support occurs. As discussed by Alexeev et al. [60], an electron transfer can be expected to take place from Ti^{3+} to Pt, if the Pt atoms and Ti^{3+} cations were to interact with each other. Similarly, Boccuzzi et al. [13] observed a band at 1960 cm^{-1} after CO adsorption on a reduced Au/TiO_2 catalyst. The low frequency of this band, which was almost completely depleted after admission of oxygen, was attributed to electron transfer from the reduced-titania support to the gold particles. On these grounds, the band at 1945 cm^{-1} is tentatively assigned to terminal CO species adsorbed on metallic Pt in contact with Ti^{3+} ions. Such [Pt–Ti^{3+}] sites are expected to be present under a reducing atmosphere at the metal–support interface. Furthermore, the population of these sites is expected to increase under conditions that favor decoration of Pt by TiO_x suboxides [60], as dictated by the SMSI effect [32,33].

Apart from the carbonyl bands discussed above, interaction of CO with the Pt/TiO_2(PC) catalyst at temperatures above 25 °C results in the progressive development of two negative bands located at 3727 and 3665 cm^{-1} (Fig. 8) that characterize OH stretching modes of two types of different surface hydroxyl groups [55,56,61]. These (negative) bands develop in parallel with peaks located at ca. 1690, 1566, and 1384 cm^{-1} that can be attributed to surface formate species associated with the support [62]. Qualitatively similar results have been reported for Pd/TiO_2 [50], Pd/CeO_2 [50], and Pt/CeO_2 [19] catalysts. It is therefore reasonable to suggest that the hydroxyl groups originally present on the catalyst surface interact with incoming CO to yield formates. The population of formates increases

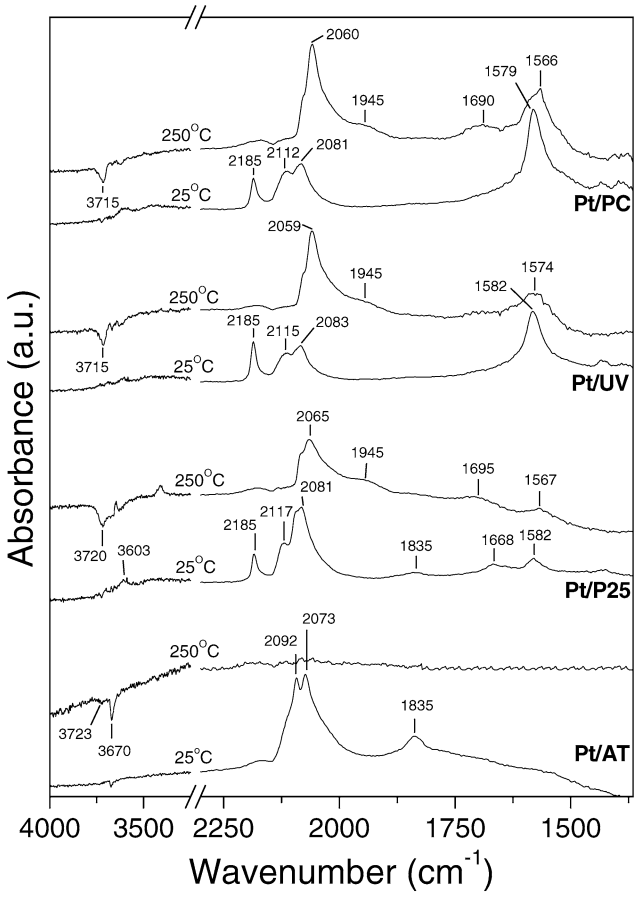

Fig. 9. DRIFT spectra obtained at 25 and 250 °C from the preoxidized Pt/TiO_2 catalysts under conditions similar to those of Fig. 8.

progressively with increasing temperature and goes through a maximum at ca. 250–300 °C (traces f and g). It should be noted that bands attributable to carbonate species can be also distinguished at ca. 1625 and 1525 cm^{-1}. At higher temperatures, the intensities of the formate and carbonate bands start to decrease and disappear above 400 °C (traces i and j). This behavior is likely due to decomposition of formates toward H_2 and CO_2 (or carbonates), and is in excellent agreement with the results of CO-TPR experiments (Fig. 7).

FTIR experiments similar to those shown in Fig. 8 were conducted for all Pt/TiO_2 catalysts investigated; representative spectra recorded at 25 and 250 °C are compared in Fig. 9. The following statements about the spectra obtained at 25 °C can be made: (a) The relative intensities of bands in the ν(CO) region attributed to CO adsorbed on PtO (2112–2117 cm^{-1}) and $Pt^{\delta+}$ (2081–2092 cm^{-1}) are lower over the low-surface area catalysts (Pt/AT and Pt/P25), compared with those over the high-surface area (low d_{TiO_2}) samples (Pt/UV and Pt/PC). Note that bands assigned to linear (2055–2069 cm^{-1}) and bridge-bonded (1835 cm^{-1}) CO on reduced Pt^0 sites appear only over the low-surface area catalysts (Pt/AT and Pt/P25). This is in agreement with the TPR results of Figs. 2 and 7, which show that the intensity of the LT peak, which corresponds to a reduction of PtO_x species, increases with increasing the surface area of the support (Table 2); and (b) the intensities of bands attributed to species adsorbed on titania, such as Ti^{4+}–CO (2185 cm^{-1}) and formates/carbonates (1700–1350 cm^{-1}) decrease with decreasing surface area of the catalyst and are practically absent in the lowest-surface area sample (Pt/AT).

Regarding the spectra obtained at 250 °C, it is of interest to note that the band at ca. 1945 cm^{-1}, which has been tentatively attributed to CO adsorbed on [Ti^{3+}–Pt] sites, is present in the spectra of all catalysts investigated, with the exception of the low-surface area Pt/At sample, for which all bands in the ν(CO) region disappeared at temperatures below 250 °C. Finally, the negative bands in the ν(OH) region are present in all spectra, indicating that the interaction of gas-phase CO with the hydroxyl groups of the support is operable for all Pt/TiO_2 samples.

3.6. Mechanistic implications

Results of kinetic measurements shown in Fig. 1 clearly show that the WGS activity of Pt/TiO_2 catalysts depends strongly on the type of the titanium dioxide powder used as support. In our previous studies, we found that the specific reaction rate (TOF) does not depend on metal loading, dispersion, or crystallite size for all metal–support combinations investigated [24,25]. As a result, the differences observed in the catalytic activity of the present Pt/TiO_2 catalysts should be attributed solely to differences in the physicochemical properties of the support. Because all samples consist of TiO_2 in its anatase form, with the exception of Pt/TiO_2(P25), which contains 25% rutile (Table 1), it is reasonable to suggest that the parameters that mainly affect catalytic activity are related to the SSA or, equivalently, to the primary crystallite size of titanium dioxide.

TPR experiments conducted over the preoxidized Pt/TiO_2 catalysts show that titanium dioxide is partly reduced at elevated temperatures when either H_2 or CO is used as the reducing agent, as evidenced by the presence of the HT peaks in Figs. 2 and 7, respectively. Comparing the intensity and the onset temperature of the HT reduction peaks, which are measures of the reducibility of the support, clearly shows that reducibility increases with increasing (decreasing) surface area (crystallite size) of titanium dioxide. This has been verified by the results of Raman experiments, which proved that formation of substoichiometric TiO_x species begins at lower temperatures and is more facile over Pt/TiO_2 catalysts with smaller titania particle sizes (Figs. 4–6). For example, formation of Ti_2O_3 is first detected for the Pt/UV sample at temperatures as low as 150 °C (Fig. 4).

In view of the above results, we propose that the WGS activity of the present Pt/TiO_2 catalysts is related to the particle size-dependent reducibility of the titania support. In particular, activity increases with increasing reducibility of TiO_2. This is in general agreement with the results of our previous investigation, which showed that the catalytic activity of Pt and Ru catalysts increases by 1–2 orders of magnitude when supported on "reducible" (TiO_2, CeO_2, La_2O_3, and YSZ) rather than on "irreducible" (Al_2O_3, MgO, and SiO_2) metal oxides [25]. Similarly, Erdohelyi et al. [63] found that the specific activity of Ir catalysts for the WGS reaction depends on the nature of the metal oxide carrier used and increases by more than one order

of magnitude when supported on TiO_2 rather than on Al_2O_3, MgO, or SiO_2. The effect of reducibility of the support on the WGS activity has been recently addressed by Fu et al. [20], who proposed that for ceria-supported metal catalysts, the role of the metal is restricted to increasing the reducibility of the support, thereby creating active sites. Similarly, Goguet et al. [23] proposed that under reaction conditions, a limited fraction of the support close to the metal particles could be in a highly reduced state and would correspond to the active state of the support.

The present results do not provide direct mechanistic information on the effect of the reducibility of the support on the WGS activity of Pt/TiO_2 catalysts. However, strong evidence is provided that the support is involved in the WGS mechanism either directly, via the regenerative (redox) mechanism, or indirectly, via the associative mechanism. If the redox mechanism is operable, then reaction steps similar to those proposed for the ceria-mediated redox process [7–11] may be considered,

$$x\mathrm{Pt} + x\mathrm{CO} \leftrightarrow x\mathrm{Pt\text{–}CO}, \tag{9}$$

$$x\mathrm{Pt\text{–}CO} + \mathrm{TiO_2} \leftrightarrow x\mathrm{CO_2} + \mathrm{TiO_{2-}}_x + x\mathrm{Pt}, \tag{10}$$

and

$$x\mathrm{H_2O} + \mathrm{TiO_{2-}}_x \leftrightarrow \mathrm{TiO_2} + x\mathrm{H_2}. \tag{11}$$

According to this scheme, the titania surface is subjected to successive reduction and oxidation steps by adsorbed CO and water, respectively, thereby cycling between TiO_{2-x} and TiO_2. Results of TPR (Figs. 2 and 7) and Raman (Figs. 3–6) experiments clearly show that titania can be reduced by H_2 or CO at temperatures as low as 150 °C. In addition, results found in the literature show that TiO_{2-x} can be reoxidized by water, according to Eq. (11). For example, Lu et al. [64] investigated the creation and reactivity of surface oxygen vacancies by thermal annealing of $TiO_2(110)$ surface and found that Ti^{3+} sites react reductively with D_2O, $^{13}CH_2O$, or ^{15}NO to produce D_2, $^{13}C_2H_4$, or $^{15}N_2O$, respectively. The authors proposed that the net result of the reaction of two Ti^{3+} active sites with water is oxidation of the former to Ti^{4+} and filling of the missing lattice oxygen [64]. Therefore, in principle, the redox mechanism described by Eqs. (9)–(11) may be operable under the present reaction conditions, if the rate of reoxidation of TiO_{2-x} by water is sufficiently rapid.

On the other hand, the beneficial effect of the reducibility of the support on the WGS activity of Pt/TiO_2 catalysts may be also explained by evoking the associative mechanism. In this case, it is has been suggested that the reaction proceeds via intermediate production of a bidentate formate species [14,15], which may be produced by interaction between CO adsorbed on platinum with hydroxyl groups of TiO_2 at the metal–support interface,

$$\mathrm{CO_{(Pt)}} + \mathrm{OH_{(TiO_2)}} \rightarrow \mathrm{HCOO_{(Pt/TiO_2)}}. \tag{12}$$

This is supported by the FTIR results of the present study, which show that CO interacts with surface OH groups at temperatures above 75 °C, yielding formate (Fig. 8). In the next step, formate species decompose to yield hydrogen atoms adsorbed on platinum and CO_2, which either desorbs immediately in the gas phase or remains bonded to the support in the form of carbonates,

$$\mathrm{HCOO_{(Pt/TiO_2)}} \rightarrow \mathrm{H_{(Pt)}} + \mathrm{CO_{2(TiO_2)}}. \tag{13}$$

Finally, adsorbed hydrogen atoms and carbonates desorb to produce gas-phase H_2 and CO_2,

$$2\mathrm{H_{(Pt)}} \rightarrow \mathrm{H_2} \tag{14}$$

and

$$\mathrm{CO_{2(TiO_2)}} \rightarrow \mathrm{CO_2}. \tag{15}$$

It may be argued that in the associative mechanism described above [Eqs. (12)–(15)], the effect of the reducibility of the support on the WGS activity is indirect and influences the population of active OH groups, which, as proposed in the case of ceria-based samples, increases with increasing degree of surface reduction of the support [14]. Jacobs et al. [17] showed that active OH groups are formed after reduction of the ceria surface cell, a process catalyzed by the presence of the dispersed metal. If we assume that the same surface processes occur over TiO_2-based catalysts, then the active OH group density is expected to depend on the degree of reduction of the titania surface. In this case, activity will increase with increasing reducibility (decreasing primary particle size) of the support, in agreement with the present results.

It becomes evident that the observed effect of the particle size-dependent reducibility of TiO_2 on the WGS activity of Pt/TiO_2 catalysts may be explained by considering either the regenerative or associative reaction mechanisms. In both cases, the presence of partially reduced titania particles in the vicinity of dispersed platinum seems to be necessary for the production of active sites at the metal–support interface. Clearly, detailed mechanistic studies are needed to further investigate the elementary steps of the WGS reaction at the Pt/TiO_2 catalyst surface.

4. Conclusion

The H_2-TPR profiles of preoxidized Pt/TiO_2 catalysts are characterized by an LT peak at ca. 200 °C, attributed to reduction of PtO_x, and by a broad feature above 300 °C, due to surface reduction of titanium dioxide toward TiO_x. The reducibility of titania, which is reflected in the onset temperature and intensity of the HT TPR feature, increases with increasing SSA of the catalyst or, conversely, decreasing primary particle size (d_{TiO_2}) of the support. This has been proven by the results of in situ Raman experiments conducted under hydrogen flow demonstrating that formation of substoichiometric TiO_x species starts at lower temperatures and is more facile over Pt/TiO_2 catalysts with smaller titania particle sizes. The results of CO-TPR experiments were qualitatively similar, demonstrating that reduction of both PtO_x and TiO_2 may be accomplished with the use of carbon monoxide as the reducing agent. The presence of an additional CO_2 peak located at intermediate temperatures, in all cases accompanied by evolution of gas-phase H_2, indicates that Pt/TiO_2 catalysts are able to oxidize CO to CO_2 via the WGS reaction. FTIR experiments provide

evidence that the reaction occurs via interaction between CO and hydroxyl groups of the support, with intermediate production of formates. Partial reduction of the support results in the creation of new sites for CO adsorption, probably located at the metal–support interface, which have been tentatively assigned to metallic Pt in contact with Ti^{3+} ions. The observed enhancement of the WGS activity of Pt/TiO_2 catalysts with increasing the reducibility of the support (decreasing d_{TiO_2}) may be explained by both the "regenerative" and the "associative" reaction mechanisms.

Acknowledgments

This work is funded in part by the General Secretariat of Research and Technology (GSRT) Hellas and the Commission of the European Community, under the PENED 2001 Program (contract 01ED561).

References

[1] D.L. Trimm, Z.I. Önsan, Catal. Rev. 43 (2001) 31.
[2] A.F. Ghenciu, Curr. Opin. Solid State Mater. Sci. 6 (2002) 389.
[3] M.V. Twigg, Catalyst Handbook, second ed., Wolfe Publishing, London, 1989, chap. 6.
[4] D.S. Newsome, Catal. Rev.-Sci. Eng. 21 (1980) 275.
[5] J.M. Zalc, D.G. Löffler, J. Power Sources 111 (2002) 58.
[6] J. Barbier Jr., D. Duprez, Appl. Catal. B 3 (1993) 61.
[7] H. Cordatos, T. Bunluesin, J. Stubenrauch, J.M. Vohs, R.J. Gorte, J. Phys. Chem. 100 (1996) 785.
[8] T. Bunluesin, R.J. Gorte, G.W. Graham, Appl. Catal. B 15 (1998) 107.
[9] S. Hilaire, X. Wang, T. Luo, R.J. Gorte, J. Wagner, Appl. Catal. A 215 (2001) 271.
[10] X. Wang, R.J. Gorte, J.P. Wagner, J. Catal. 212 (2002) 225.
[11] R.J. Gorte, S. Zhao, Catal. Today 104 (2005) 18.
[12] Y. Li, Q. Fu, M. Flytzani-Stephanopoulos, Appl. Catal. B 27 (2000) 179.
[13] F. Boccuzzi, A. Chiorino, M. Manzoli, D. Andreeva, T. Tabakova, J. Catal. 188 (1999) 176.
[14] T. Shido, Y. Iwasawa, J. Catal. 141 (1993) 71.
[15] G. Jacobs, L. Williams, U. Graham, D. Sparks, B.H. Davis, J. Phys. Chem. B 107 (2003) 10398.
[16] G. Jacobs, L. Williams, U. Graham, G.A. Thomas, D.E. Sparks, B.H. Davis, Appl. Catal. A 252 (2003) 107.
[17] G. Jacobs, E. Chenu, P.M. Patterson, L. Williams, D. Sparks, G. Thomas, B.H. Davis, Appl. Catal. A 258 (2004) 203.
[18] G. Jacobs, U.M. Graham, E. Chenu, P.M. Patterson, A. Dozier, B.H. Davis, J. Catal. 229 (2005) 499.
[19] G. Jacobs, P.M. Patterson, U.M. Graham, A.C. Crawford, B.H. Davis, Int. J. Hydrogen Energy 30 (2005) 1265.
[20] Q. Fu, H. Saltsburg, M. Flytzani-Stephanopoulos, Science 301 (2003) 935.
[21] Q. Fu, S. Kurdiavtseva, H. Saltsburg, M. Flytzani-Stephanopoulos, Chem. Eng. J. 93 (2003) 41.
[22] Q. Fu, W. Deng, H. Saltsburg, M. Flytzani-Stephanopoulos, Appl. Catal. B 56 (2005) 57.
[23] A. Goguet, F. Meunier, J.P. Breen, R. Burch, M.I. Petch, A.F. Chenciu, J. Catal. 226 (2004) 382.
[24] P. Panagiotopoulou, D.I. Kondarides, J. Catal. 225 (2004) 327.
[25] P. Panagiotopoulou, D.I. Kondarides, Catal. Today 112 (2006) 49.
[26] T. Chafik, D.I. Kondarides, X.E. Verykios, J. Catal. 190 (2000) 446.
[27] D.I. Kondarides, T. Chafik, X.E. Verykios, J. Catal. 191 (2000) 147.
[28] T. Huizinga, J. van Grondelle, R. Prins, Appl. Catal. 10 (1984) 199.
[29] H.C. Yao, M. Steg, H.K. Plumer Jr., J. Catal. 59 (1979) 365.
[30] C.-P. Hwang, C.-T. Yeh, J. Mol. Catal. A 112 (1996) 295.
[31] J.Z. Shyu, K. Otto, J. Catal. 115 (1989) 16.
[32] S. Tauster, S.C. Fung, L. Garten, J. Am. Chem. Soc. 100 (1978) 170.
[33] G.L. Haller, D.E. Resasco, Adv. Catal. 36 (1989) 173.
[34] T. Huizinga, R. Prins, J. Phys. Chem. 85 (1981) 287.
[35] J.P. Conesa, J. Soria, J. Phys. Chem. 86 (1982) 1392.
[36] P. Gajardo, T.M. Apple, C. Dybowski, Chem. Phys. Lett. 74 (1980) 306.
[37] H. Cordatos, D. Ford, R.J. Gorte, J. Phys. Chem. 100 (1996) 18128.
[38] E.S. Putna, B. Sherek, R.J. Gorte, Appl. Catal. B 17 (1998) 101.
[39] A. Trovarelli, Catal. Rev.-Sci. Eng. 38 (1996) 439.
[40] A. Trovarelli, C. de Leitenburg, G. Polcetti, J. Llorca, J. Catal. 151 (1995) 111.
[41] Y.M. Chiang, E.B. Lavik, I. Kosacki, H.L. Tuller, J.Y. Ying, J. Electroceram. 1 (1997) 7.
[42] J.C. Parker, R.W. Siegel, Appl. Phys. Lett. 57 (1990) 943.
[43] A. Mooradian, P.M. Raccah, Phys. Rev. B 3 (1971) 4253.
[44] S.H. Shin, R.L. Aggawal, B. Lax, J.M. Honig, Phys. Rev. B 9 (1974) 583.
[45] A. Perez del Pino, P. Serra, J.L. Morenza, Thin Solid Films 415 (2002) 201.
[46] A. Perez del Pino, P. Serra, J.L. Morenza, Appl. Surf. Sci. 197–198 (2002) 887.
[47] E. Gyorgy, A. Perez del Pino, P. Serra, J.L. Morenza, Appl. Surf. Sci. 222 (2004) 415.
[48] S.D. Jackson, N.M. Glanville, J. Willis, G.D. McLellan, G. Webb, R.B. Moyes, S. Simpson, P.B. Wells, R. Whyman, J. Catal. 139 (1993) 207.
[49] A. Martinez-Arias, J.M. Coronado, R. Cataluna, J.C. Conesa, J. Soria, J. Phys. Chem. B 102 (1998) 4357.
[50] H. Zhu, Z. Qin, W. Shan, W. Shen, J. Wang, J. Catal. 225 (2004) 267.
[51] C. Serre, F. Garin, G. Belot, G. Maire, J. Catal. 141 (1993) 1.
[52] D.G. Rethwisch, J.A. Dumesic, Langmuir 2 (1986) 73.
[53] F. Boccuzzi, A. Chiorino, S. Tsubota, M. Haruta, J. Phys. Chem. 100 (1996) 3625.
[54] P. Konova, A. Naydenov, Cv. Venkof, D. Mehandjiev, D. Andreeva, T. Tabakova, J. Mol. Catal. A 213 (2004) 235.
[55] G. Busca, H. Saussey, O. Saur, J.C. Lavalley, V. Lorenzelli, Appl. Catal. 14 (1985) 245.
[56] K. Hadjiivanov, J. Lamotte, J.C. Lavalley, Langmuir 13 (1997) 3374.
[57] M. Primet, J.M. Basset, M.V. Mathieu, M. Prettre, J. Catal. 29 (1973) 213.
[58] M. Primet, J. Catal. 88 (1984) 273.
[59] P.-A. Carlsson, L. Österlund, P. Thormählen, A. Palmqvist, E. Fridell, J. Jansson, M. Skoglundh, J. Catal. 226 (2004) 422.
[60] O.S. Alexeev, S.Y. Chin, M.H. Engelhard, L. Ortiz-Soto, M.D. Amiridis, J. Phys. Chem. B 109 (2005) 23430.
[61] F. Boccuzzi, A. Chiorino, J. Phys. Chem. 100 (1996) 3617.
[62] T. Kecskés, J. Raskó, J. Kiss, Appl. Catal. A 273 (2004) 55.
[63] A. Erdohelyi, K. Fodor, G. Suru, Appl. Catal. A 139 (1996) 131.
[64] G. Lu, A. Linsebigler, J.T. Yates Jr., J. Phys. Chem. 98 (1994) 11733.